

Direct Numerical Simulation of Wetting and Spreading Behavior on Heterogeneous and Roughened Substrates

Leonard W. Schwartz, Departments of Mechanical Engineering and Mathematical Sciences, University of Delaware, Newark, DE 19716, USA, schwartz@me.udel.edu

ABSTRACT

A method of calculation is presented that allows the simulation of the time-dependent three-dimensional motion of thin liquid layers on solid substrates for systems with finite equilibrium contact angles. The contact angle is a prescribed function of position on the substrate. Similar mathematical models are constructed for substrates with a pattern of roughness. Evolution equations are given, using the lubrication approximation, that include viscous, capillary and disjoining forces. Motion to and from dry substrate regions is made possible by use of a thin energetically-stable wetting layer. We simulate motion on heterogeneous substrates with periodic arrays of high contact-angle patches. Two different problems are treated for heterogeneous substrates. The first is spontaneous motion driven only by wetting forces. If the contact-angle difference is sufficiently high, the droplet can find several different stable positions, depending on the previous history of the motion. A second simulation treats a forced cyclical motion. Energy dissipation per cycle for a heterogeneous substrate is found to be larger than for a uniform substrate with the same total energy. The Landau-Levich solution for plate removal from a liquid bath is extended to account for a pattern of roughness on the plate.

1. INTRODUCTION

Wetting and capillary considerations during the slow motion of liquids on solid substrates are important in both the technological and natural worlds. Applications include the spreading behavior of liquid coatings, as well as flows in oil reservoirs, chemical reactors and heat exchangers. Some biological application areas are motions in the tear film on the cornea of the eye, flows on liquid covered membranes in the lungs, and the general area of cell motility, where cell motions have many of the features of inert liquid droplets [1]. The spreading properties of agrochemicals such as pesticides and insecticides are important determinants of their effectiveness. Capillary forces are often dominant in problems of small physical dimensions; however they can also be important for large-scale phenomena when body forces

are very weak, as in the microgravity environment of orbiting satellites in space.

Application of a wettability pattern or a pattern of roughness to the walls of vessels containing liquid is a possible strategy for controlling the position of the liquid in the microgravity environment of orbiting space vehicles. In the absence of gravity, liquid in a partially-filled container can assume many different configurations. Small imposed accelerations can cause large displacements of the liquid which is undesirable for a variety of reasons. Contact line dynamics will play an important role, either by "pinning" the location of the liquid on the wall or by dissipating the kinetic energy imparted to the liquid. The present results suggest that different wall wettability patterns may accomplish one or the other of these objectives.

We will briefly outline mathematical and numerical procedures for liquid motions on chemically heterogeneous or roughened substrates. These employ the long-wave or "lubrication" approximation. More complete information can be found elsewhere [2,3,4].

2. THE MATHEMATICAL MODEL

Integral mass conservation is

$$h_t = -\nabla \cdot \mathbf{Q} + w_i(x, y, t) \quad (2.1)$$

Here h is the thickness of the liquid layer and \mathbf{Q} is the two-dimensional areal flux vector defined as

$$\mathbf{Q} = \int_0^{h(x,y)} (u, v) dz$$

where u and v are velocity components in the x and y directions respectively. Likewise ∇ is a two-dimensional operator with respect to x and y . w_i is a local injection rate that is an input function of substrate position and time.

Under the assumptions of lubrication theory [5,6], i.e. the motion is sufficiently slow that inertial forces may be neglected and the free surface is inclined at a small angle relative to the substrate, the momentum equation for an assumed Newtonian liquid may be integrated

to yield

$$\mathbf{Q} = -\frac{1}{3\mu}(h^3\nabla p). \quad (2.2)$$

Here μ is the viscosity and the pressure p is independent of the normal coordinate z . The no-slip condition for the velocity has been applied on the substrate and the liquid free surface is stress-free. The pressure in the liquid is given by

$$p = -\sigma\kappa - \Pi \approx -\sigma\nabla^2 h - \Pi \quad (2.3)$$

and the pressure above the liquid is taken to be zero without loss of generality. The first term on the right is an approximation to the free-surface curvature when the surface slope is small. The error in this curvature approximation is proportional to the square of the surface inclination. σ is surface tension and the so-called disjoining pressure is given by the two-term model [2,3,7]

$$\Pi = B \left[\left(\frac{h^*}{h} \right)^n - \left(\frac{h^*}{h} \right)^m \right]. \quad (2.4)$$

B and the exponents n and m are positive constants with $n > m > 1$. The local disjoining energy density

$$e^{(d)}(h) = - \int_{h_*}^h \Pi(h') dh' \quad (2.5)$$

has a single stable energy minimum at the thin wetting-layer thickness $h = h_*$. A local force balance near an apparent contact line gives

$$\sigma \cos \theta_c = \sigma - e^{(d)}(\infty) \quad (2.6)$$

which is the disjoining-model equivalent of the Young-Laplace equation.

The equilibrium contact angle is taken to be an arbitrarily prescribed function of position and the evolution equation for flow over a heterogeneous substrate becomes

$$h_t = -\frac{\sigma}{3\mu} \nabla \cdot \left[h^3 (\nabla \nabla^2 h + \frac{(n-1)(m-1)}{2h_*(n-m)} \nabla \left[\theta_c^2 \left(\frac{h_*^n}{h^n} - \frac{h_*^m}{h^m} \right) \right] \right) \right] + w_i(x, y, t) \quad (2.7)$$

It is possible to augment this equation with gravity and other force terms as additional driving mechanisms. [3]

Each pressure component on the right of equation (2.3) may be identified with an integrated energy component. The free-surface energy is proportional to the area of the liquid surface and is given by

$$E^{(\sigma)} = \sigma \iint \left(\frac{1}{\cos \gamma} - 1 \right) dA \approx \frac{\sigma}{2} \iint \nabla h \cdot \nabla h dA \quad (2.8)$$

where A is the total area of the substrate, and γ is the angle between the normal to the surface and the normal to the substrate. The total disjoining energy is

$$E^{(d)} = \iint e^{(d)} dA. \quad (2.9)$$

The global energy change equation is

$$\dot{E}^{(\mu)} = -(\dot{E}^{(\sigma)} + \dot{E}^{(d)}) + \dot{\mathbb{W}} \quad (2.10)$$

which is the statement that the rate of viscous working is equal to the rate of decrease of the stored, or potential, energy components plus the rate of working on the system. Here

$$\dot{\mathbb{W}} = \iint p w_i dA \quad (2.11)$$

may be recognized as the rate of working on the system by means of injection w_i . For cyclical motions, the drop shape returns to its original configuration and there is no change, over a cycle, in $E^{(\sigma)}$ or $E^{(d)}$. In that case the total viscous work done is the time integral of $\dot{\mathbb{W}}$ or

$$\oint p dV$$

where V is drop volume, $dV = w_i dA$ and the special integral sign denotes a full cycle.

For the quasi-three dimensional problems treated here, numerical solutions use finite difference methods and an alternating direction implicit (ADI) technique is implemented. Developed originally for second-order elliptic and parabolic systems [8], ADI uses alternating sweeps in each direction and only a banded system of equations needs to be solved to update the discrete set of $h_{i,j}$ values.

3. VALIDATION

The model has been calibrated by comparison with several experiments. Axisymmetric spreading of a droplet on a high-energy [i.e. small contact angle] uniform substrate has been measured by several investigators and general agreement with Tanner's Law [9]

$$A \propto V^{-3/5} t^{1/5}$$

has been verified. Here A is drop area, V is volume and t is time. It can be shown that the solution for $h(r, t)$ is self-similar and the drop central height must also follow a power law in time [3]. Figure 1 shows a comparison of the similarity solution assuming a wetting layer of 30 nm thickness which agrees with experimental results [10]. Also shown is an axisymmetric simulation on a uniform low-energy substrate with a finite contact angle. It is seen that the power-law is followed until the drop has almost stabilized at a dimensionless central height $h_c \approx 1$. This spreading behavior, with finite contact angle, has been observed experimentally by Zosel [11]. Another simulation, shown as symbols in the Figure, assumes the substrate has a pattern of wettability as in Fig. 5. The substrate area-average wettability is the same as for the low-energy uniform case. It can be seen that the spreading is unaffected by the contamination pattern until the droplet slows and ultimately stops spreading. Three-dimensional simulations are limited to thick precursor layers because of the need to adequately resolve details in the contact region. Too thick a precursor layer results in a relatively weak speed discrepancy; this discrepancy is in accordance with the predicted inverse logarithmic dependence on the precursor thickness [12].

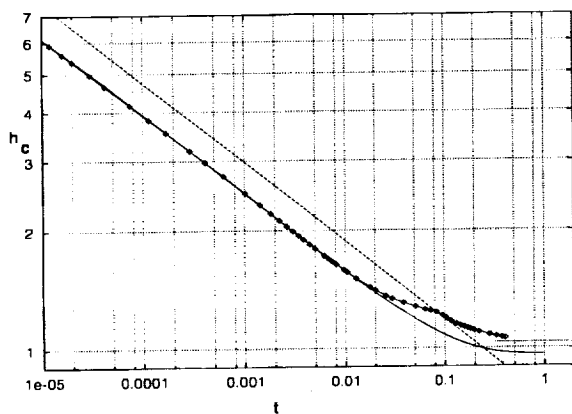


Figure 1: Drop central height h_c versus time, showing the similarity range for axisymmetric spreading. The initial drop height is 10. The straight line on this log-log plot is $h_c = 0.75t^{1/5}$ which matches experiments. The solid curve is the calculated behavior for finite contact angle on a uniform substrate, while the lines-points curve is calculated for the square wettability pattern.

We have performed a laboratory experiment to compare with drop spreading simulations [3]. A 26 μl drop of glycerin was placed near the center of a cross of 1

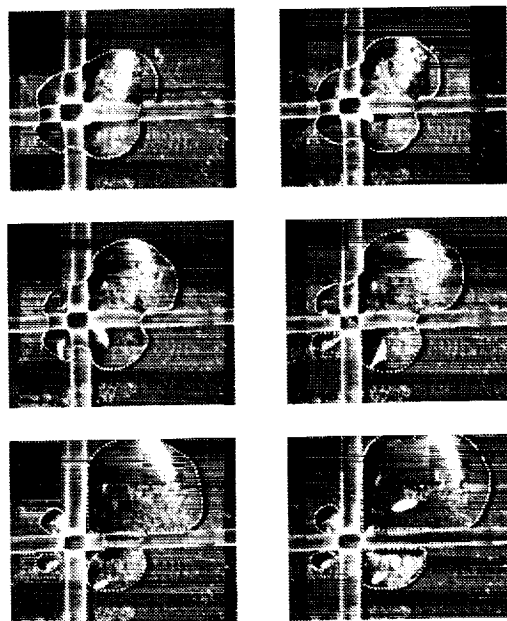


Figure 2: Video images taken from an experiment where a glycerin drop is placed near the center of a cross of 0.1 cm Teflon tape on a glass slide. These pictures may be compared with the simulation shown in Fig. 3.

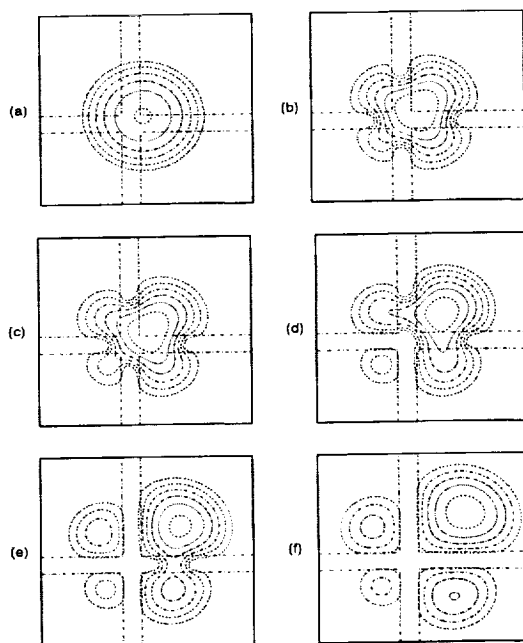


Figure 3: Contour plots from a computer simulation of break-up of a liquid drop placed on a "cross" of high-contact-angle material.

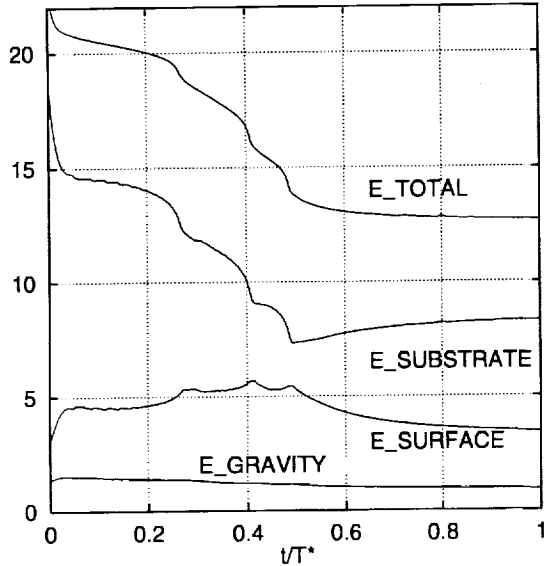


Figure 4: Energy components versus time from the drop-on-cross simulation.

mm Teflon tape that had been fixed to a horizontal glass slide. Wetting forces cause the drop to break up into unequal fragments as shown in Fig. 2. Simulation results, in Fig. 3, show detailed agreement with the experiment. However time-scale corrections need to be applied because (i) the simulation precursor layer is overly large, and (ii) the contact angles in the experiment are beyond the range of quantitative validity of the small-slope lubrication approximation. Energy component variation, from the simulation, is given in Fig. 4. The Bond number $Bo = \rho g R^2 / \sigma = 2.5$ using the stabilized radius R for the drop on glass. The gravitational effect is quite minor, however, as can be seen in the Figure. Note that the motion proceeds in a “jerky” manner that is characteristic of capillary driven motions on nonuniform substrates. Each drop disconnection is reflected as a rapid decrease in the substrate energy.

4. HYSTERETIC MOTIONS ON HETEROGENEOUS SURFACES

Simulations have been performed to investigate the dissipation of energy when a liquid moves on mixed-wettable substrates. Again we consider the motion of a drop, both in spontaneous motion, driven only by wetting forces, and also in a periodic forced motion. Several periodic patterns of wettability have been consid-

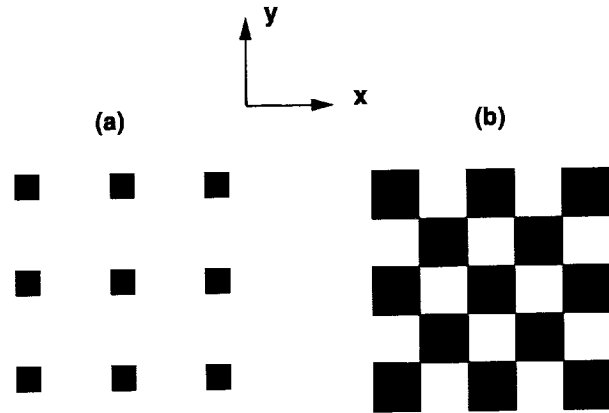


Figure 5: The substrate wettability patterns used in this study. The dark regions have larger values of contact angle than the surrounding field. (a) Isolated spot pattern; (b) Checkerboard pattern.

ered, two of which are shown in Fig. 5. The equilibrium contact angle θ_e is larger on the dark patches than on the surrounding field. Numerical procedures for generating these and other patterns, including slight smoothing at patch boundaries to maintain derivative continuity, are given in [2].

Figure 6 shows two different stable drop shapes obtained by allowing a drop to advance outward (left) and recede (right) from a starting profile that was either steeper or shallower than the equilibrium shapes. The contact angle on the isolated patches is about four times larger than on the field. Effective advancing and receding contact angles may be calculated using averages of local values; the effective contact angle ratio for this case is $\theta_a / \theta_r = 1.14$. This ratio is a measure of contact angle hysteresis. Figure 7 is an instantaneous picture during the receding simulation. It shows transient interior dewetting due to an instability near the receding contact line.

A schematic diagram for a notional experiment to explore energy dissipation in forced motions is shown in Fig. 8. By pumping liquid in and out via a syringe, the droplet can be forced to periodically traverse the wettability pattern. Pressure-volume plots from numerical simulation are shown in Fig. 9 where motions on a checkerboard wettability pattern are compared with a uniform substrate of the same average energy. The area of each hysteresis loop is the input work required to drive a cycle of the motion. Additional dissipation results from the presence of the pattern, the effect being more important at low speeds or long cycle times.

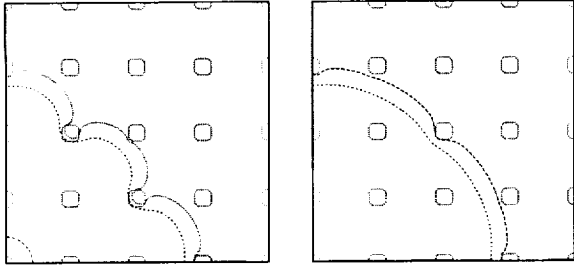


Figure 6: Contour plots of final static shapes for advanced (left) and receded (right) drops in spontaneous motion. The wettability pattern is also shown. The difference between the two cases is a measure of contact angle hysteresis.

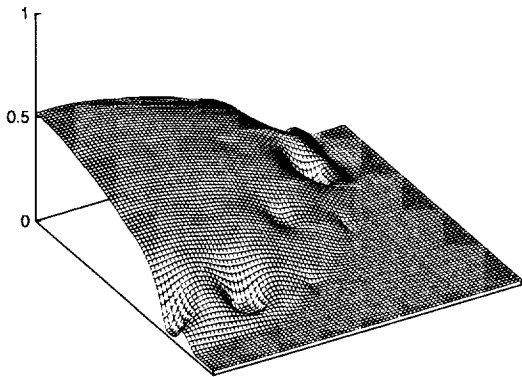


Figure 7: A frame during recede. A de-wetting instability leads to interior dry patches near the receding periphery. This is a transient effect and the drop continues to recede until the final configuration, shown in Fig. 6, is attained.

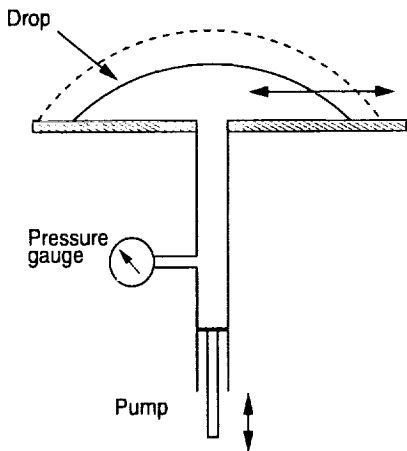


Figure 8: Schematic diagram of a notional experiment to investigate energy dissipation in a cyclic motion of a drop.

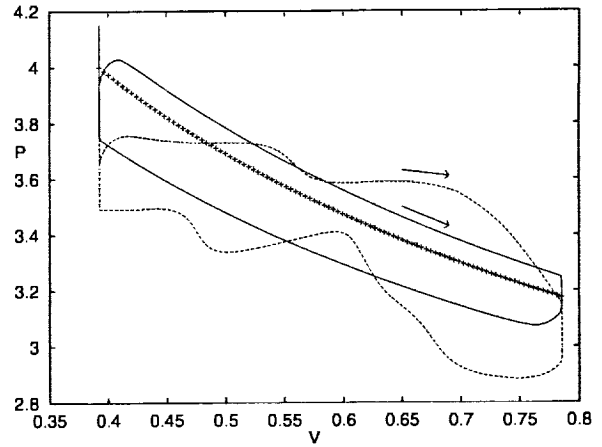


Figure 9: Dimensionless pressure P versus volume V showing hysteresis loops in cyclical motion. The solid line is for a uniform substrate, dashed line is for a checkerboard wettability pattern. The symbol curve is for the non-dissipative quasi-static theory with equation $P = 2\pi^{1/3}V^{-1/3}$.

For comparison, a quasi-static non-dissipative curve, for motion on a uniform substrate, is also shown.

5. MOTIONS ON A SURFACE WITH A PATTERN OF ROUGHNESS

It is possible to include a roughened substrate in the lubrication formulation. It may be shown [4] that the evolution equation needs only be modified by inclusion of the substrate shape function in the "permeability," *i. e.* the factor of proportionality between the flux and the pressure gradient. It is often convenient to allow the substrate to move with time while the computational window is fixed to the liquid free surface.

A model problem is an extension of the well-known Landau-Levich [13] problem for the withdrawal of a moving plate from a bath of liquid. We consider the plate to have a periodic pattern of roughness or "cells" as shown in Fig. 10. The plate moves with constant speed U to the right while the liquid meniscus is pinned at the left end of the computational window. While the Landau-Levich result is time independent, here the problem becomes time periodic with a period equal to the cell passage time. All dimensional constants can be absorbed by scaling. We let h_0 be a measure of coating thickness, such as the cell depth and substrate coordinates (x, y) are made dimensionless using the length

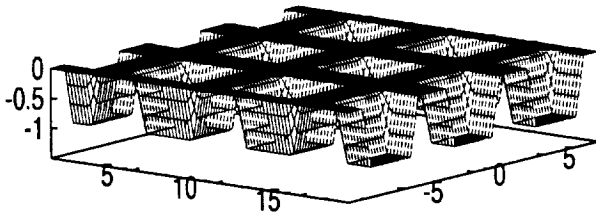


Figure 10: A periodic square array of cells on the substrate.

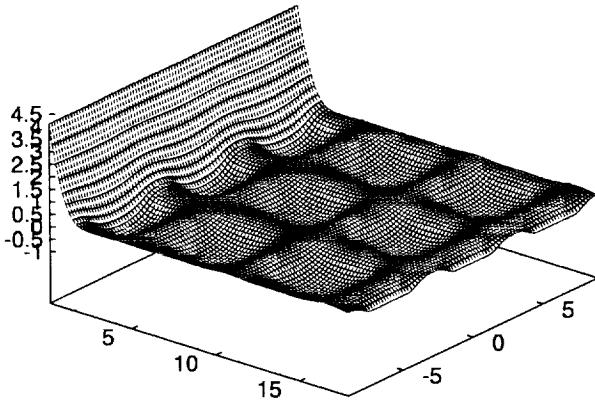


Figure 11: A liquid surface during meniscus withdrawal for the cell pattern in Fig. 10. Note how the meniscus 'scrapes out' the cells.

scale

$$L = h_0 \left(\frac{\sigma}{3\mu U} \right)^{1/3} \quad (5.1a)$$

The time unit is

$$T^* = \frac{L}{U} \quad (5.1b)$$

The long-wave model equation is

$$\frac{\partial h}{\partial t} = -\frac{\partial h}{\partial x} - \nabla \cdot (s \nabla \nabla^2 h) \quad (5.2)$$

A function $h_1(x, y, t)$ represents the moving substrate and the permeability s in (5.2) is simply $s = (h - h_1)^3$.

As seen in Fig. 11, the downward pressure of the meniscus acts so as to "scrape" liquid from the cells. A certain residual fraction remains in each cell, determined primarily by the cell geometry. Much greater work is required to move the plate compared to a smooth-wall case. The problem is applicable to damping of periodic motions where the wall roughness is a surrogate for the chemical heterogeneity discussed above. Further details, including terrestrial applications in the coating and printing industry, where engraved or "gravure" rollers are used, are given in [4].

6. ACKNOWLEDGMENT

This work is supported by the NASA Microgravity Program, ICI, and The State of Delaware.

7. REFERENCES

1. Greenspan, H. P., *J. Fluid Mechanics* **84**, 125 - 143, 1978.
2. Schwartz, L. W., *Langmuir* 1998 (in press).
3. Schwartz, L. W. & Eley, R. R., *J. Colloid Interface Sci.* 1998 (in press).
4. Schwartz, L. W., P. Moussalli, P. Campbell, & R. R. Eley *Trans. Inst. Chem. Engrs.* **76**, 22-29 (1998)
5. Atherton, R. W. & Homsy, G. M., *Chem. Eng. Comm.* **2**, 57 (1976).
6. Benney, D. J., *J. Math. & Phys.* **45**, 150 (1966).
7. Mitlin, V. S., *J. Colloid Interface Sci.* **156**, 491 (1993).
8. Peaceman, D. W. & Rachford, H. H., *SIAM J.* **3**, 28 (1955).
9. Tanner, L., *J. Phys. (D)* **12**, 1473 (1979).
10. Lelah, M. D. & Marmor, A. M., *J. Colloid Interface Sci.* **82**, 518 (1981).
11. Zosel, A., *Colloid & Polymer Sci.* **271**, 680 (1993).
12. De Gennes, P. G., *Rev. Mod. Physics* **57**, 827 (1985).
13. Kim, J. S., Kim, S., & Ma, F., *J. Appl. Phys.* **73**, 422-428, (1993).
14. Levich, V., *Physicochemical Hydrodynamics*, Prentice-Hall, Englewood Cliffs (1962).